Original scientific paper

NUMERICAL INVESTIGATION OF THE INFLUENCE OF THE LINK POSITIONING IN THE CORONARY STENT INSIDE THE NORMAL ARTERY: A COMPARATIVE STUDY OF TWO COMMERCIAL STENT DESIGNS

Chandrakantha Bekal[1], Satish Shenoy[1], Ranjan Shetty[2]

[1]Department of Aeronautical & Automobile Engineering, Manipal Institute of Technology,
Manipal Academy of Higher Education (MAHE) Manipal, India
[2]Manipal Hospitals, Bangalore, India

Abstract. *This paper investigates the performance of two commercial stent designs inside the normal artery for induced Von Mises Stress and radial displacement pattern. Investigation focuses on identifying the key design feature of the stent structure responsible for varied stress and displacement pattern. Two commercial stent designs, Supraflex (Stent S) and Yukon Choice (Stent T),are modeled using micro CT images and MIMICS® while idealized models are used for investigation. ANSYS Workbench is used to numerically expand the stent inside an idealized normal artery with inflation pressure. The stent and the artery are modeled using elastic-plastic and hyperelastic material models, respectively. The results suggest crucial influence of the link positioning in inducing an area of higher Von Mises Stress and stress gradient. The locations of a higher stress gradient are those in line with unbound stent crowns. Also, higher and uniform arterial displacement can be observed in the locations in line with the bound crown. Results also suggested a considerable difference in arterial distortion induced by two designs, causes for which can also be attributed to the differences in the link placement. The study suggests that the link connections play a crucial role in setting up stress field/radial displacement. Suitable modification of the link positioning can reduce the higher stress gradient and arterial distortion, which probably can reduce arterial injury.*

Key Words: *Coronary Stents, Finite Element Analysis, Arterial Stress, Artery Radial Displacement, Arterial Distortion*

1. INTRODUCTION

It has been reported that Cardiovascular Disease (CVD) is a major cause of mortality (about 30%) world over [1-2]. Stenosis of the coronary artery is a major health issue involving accumulation of fatty deposits thereby narrowing the lumen area leading to Myocardial Infraction (MI). Stenosis is conveniently treated using coronary stents [3]. Percutaneous Coronary Intervention (PCI) has revolutionalized the treatment of stenosis and there has been tremendous increase in the number of stents being used worldwide [1], [4]. Mechanical interaction between the stent and the artery plays a crucial role in setting up a non-physiological stress field. It is reported that higher arterial stress can lead to greater intimal thickening [5]. Smooth muscle cell proliferation and stent migration immediately post stenting can lead to narrowing of vessel, the condition known as In-Stent Restenosis [6]. Clinicians are encountered with a variety of stent designs to choose from with a variety of geometrical configurations [7]. Measuring immediate stress field post stenting is experimentally nonviable. Data about comparative advantages/disadvantages of different stent designs are seldom available since assessment of long-term efficacy of implanted stent needs a long clinical trial period. Hence a promising alternative for predicting the performance of the coronary stent is numerical investigation which has been successfully utilized to investigate different generic as well as realistic stent designs [8-10], also supported by clinical implications of design parameters [11-13]. Azaouzi et al [14], investigated the effect of 'link' on bending and torsional capabilities without considering the artery interaction and suggested that bending and torsion are greatly affected by the link shape and placement. Bukala et al [15] investigated for expansion of the stent inside the stenotic artery and discussed the mechanical interaction between stent/artery surface highlighting stress and strain pattern. Chua et al [16] investigated interaction between the stent and the balloon during expansion and discussed stress distribution on the stent surface. A paper by Bedoya et al [17] investigated the effect of the stent design parameters such as curvature radius, axial strut spacing and amplitude on biomechanical responses. Martin et al [18] investigated the influence of the balloon folding configuration on arterial stress and suggested that the balloon configuration significantly affects the stress on the stent and the artery.

Though researchers investigated stress and displacement pattern, the rationale for a particular stress field and displacement pattern as well as identification of the key design feature responsible for the same are rarely reported. In this study, we tried to identify the key components of the stent design crucial for inducing a stress field and displacement pattern. Our study investigates the comparative performance of two different stent designs using commercial Finite Element Analysis (FEA) software ANSYS workbench (Ansys Inc.). This paper involves realistic modeling of stent models in order to identify the geometrical arrangements of stent struts and links, and a numerical analysis of the expansion of the idealized stent model inside the idealized normal artery. The main outcome of the investigation is identification of the key design feature, which is responsible for differences in induced arterial Von Mises Stress (VMS) and differences in the arterial displacement pattern. The investigation findings are expected to serve as a qualitative tool to underscore the importance of the key design feature in the construction of the stent design and its clinical implications.

2. METHODS AND MATERIALS

2.1. Geometry

2.1.1. Stent

Idealized geometry of stents, *SupraflexTM (Sahajanand Medical Technologies Pvt. Ltd, INDIA)*, hereafter referred as Stent S, and *Yukon Choice PC (Translumia Therapeutics, INDIA)*, hereafter referred as Stent T, are modeled using 3D image reconstructed using Micro Computed Tomography (Xradia versa XRM500, IISc, Bangalore) and Materialize Mimics® Innovation Suite. The main dimensions of the stent models in crimped form are tabulated (Table 1).

Table 1 Crimped stent dimensions (Diameters are actual values as measured on the models)

Stent	Inner radius (mm)	Outer radius (mm)	Length (mm)	Strut thickness (mm)
Stent S	0.36	0.46	4	0.1
Stent T	0.46	0.56	4	0.1

Reconstructed models from Mimics® and idealized stent models (created by wrapping stent profile) (simplified as a rectangle section) are as shown in Figs. 1 and 2, respectively.
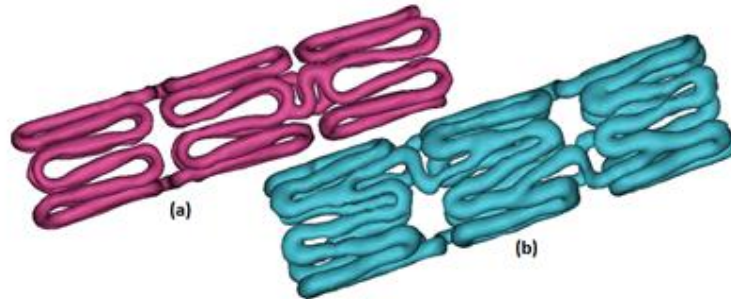

Fig. 1 3-Dimensional realistic geometry from MIMICS, Stent S (a) and Stent T (b)
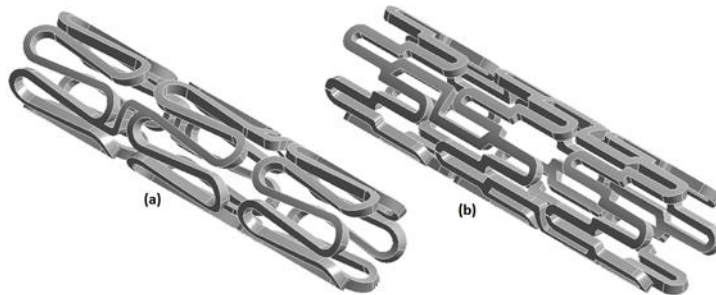
Fig. 2 Idealized geometry of Stent S (a) and Stent T (b)

2.1.2. Artery

A healthy artery is modeled as a straight cylinder with a representative dimension of 1mm inner radius and 0.4mm thickness [19]; the artery length is taken to accommodate an unstented region into its value (1mm each on each side). The stent models are centrally placed as concentric with the artery model as shown in Fig. 3.
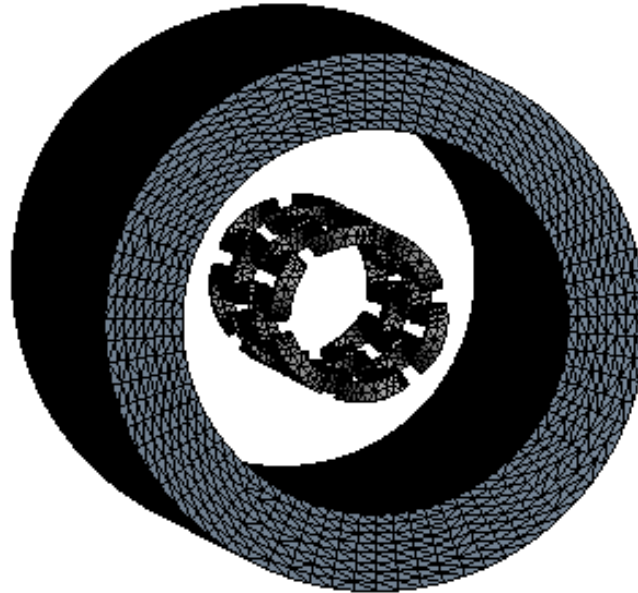
Fig. 3 Concentrically placed stent/artery meshed model (mesh size: artery-0.2mm, stent-0.05mm)

2.2. Material

Medical grade stainless steel (AISL316L) is extensively used for manufacturing a balloon expandable stent. Bilinear Elastic-Plastic material model is assumed for this class of material with properties listed in Table 2 [20-21].

Table 2 Bilinear elastic-plastic material constants used for stent modeling

Stent material	Young's modulus	Yield strength	Poison's ratio	Tangent modulus	Density
AISL316L	196GPa	205MPa	0.3	692MPa	7850kg/m^3

The artery is modeled as hyperelastic with 5 parameter Mooney-Rivlin model with constants as tabulated in Table 3 [22].

Table 3 5-parameter Mooney-Rivlin hyperelastic material constants

	Material Model	Constants	Values(KPa)
Artery	3rd order 5 parameter Mooney Rivlin	C_{10}	18.9
		C_{01}	2.75
		C_{20}	85.72
		C_{11}	590.43
		C_{02}	0

2.3. Simulation conditions

The crimped stent model is expanded in the first load step (subsequent removal of pressure in the second load step to simulate final condition, achieving final diameter of stent in the range of 1.6mm to 1.7mm) inside the idealized normal artery by 2MPa inflation pressure directly applied to the internal surface of the stent in radially outward direction [15-16]. Rigid body motion of the stent is prevented by restricting few nodes of approximately central section of the central stent cell in longitudinal and tangential direction allowing only radial movement. A Frictional contact with coefficient 0.2 is defined between the stent and the artery surface [23]. The artery ends are tethered in all directions (longitudinal, tangential and radial) to prevent a rigid body movement. A large deformation option is activated to perform a nonlinear analysis. Augmented Lagrangian contact formulation with penetration tolerance of 0.1 and normal stiffness 0.1 is used (These values specify the maximum penetration and stiffness allowed when contacts are encountered during simulation). Intraluminal pressure caused by pressurized blood and *in-vivo* longitudinal prestretch are neglected in this study.

In post processing, percentage of luminal surface subjected to critical von Mises Stress (VMS) level is identified. These critical stress level (class I>545KPa and class III>475KPa) are adapted from Ref. [17]. Apart from this, a plot of VMS gradient (Ratio of difference between VMS between two consecutive nodal points and the difference in distance between those two points) on the arterial inside surface along arbitrary paths are plotted to identify the locations of a high stress gradient [24]. Variations of radial displacement of the arterial surface through the same paths are plotted. The plots of radial displacement of the arterial inside surface at different sections, particularly to highlight the displacements near the link locations, identify distortion of the arterial inside surface post expansion. Arterial distortion is presented as difference between maximum to minimum radial displacement of the artery surface across left, central and right stent sections.

2.4. Mesh density test

Mesh density test result (Table 4) suggested a large variation in the peak VMS on the artery surface but the maximum radial displacement is unaffected by element size. We choose radial displacement as criterion for a mesh density test since the peak VMS is observed only at few nodal locations, whereas the maximum radial displacement on the artery surface prevailed over larger nodal locations. For the chosen criterion, though found to be independent of the mesh size, we chose a mesh size of 0.05mm for stent and 0.2mm for artery, respectively, with a linear tetrahedron element. Fig. 4 shows two of such meshes used for this study.

Table 4 Summary of mesh sensitivity test on artery expansion

Artery Mesh size (mm)	Stent mesh size (mm)	Peak VMS artery (MPa)	Peak VMS artery (elemental mean) (MPa)	Peak VMS stent (MPa)	Peak VMS stent (elemental mean) (MPa)	Artery displacement (max) (mm)	Stent inside Displacement (Max/Min) (mm)	Number of Nodes/Elements
0.4	0.1	0.20	0.27	263.6	254.1	0.26	0.80/0.70	83852/15519
0.2	0.1	0.39	0.50	263.8	252.9	0.27	0.81/0.70	101784/25494
0.1	0.1	0.65	0.94	263.7	252.9	0.26	0.81/0.70	173631/66601
0.08	0.05	0.88	1.35	291.5	291.1	0.26	0.80/0.70	285783/130363

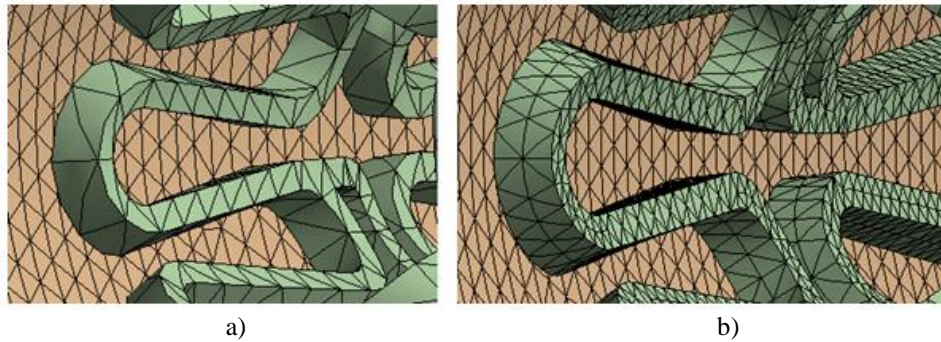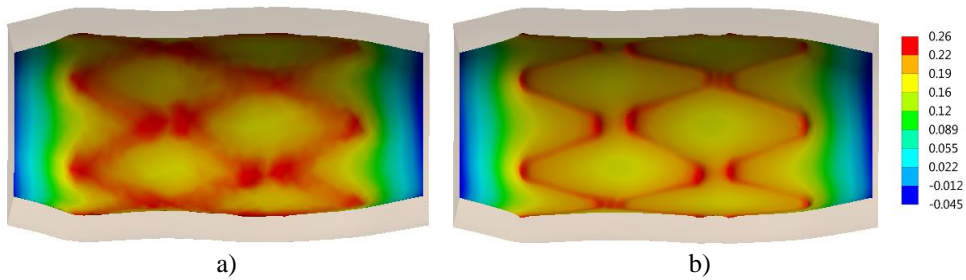a)   b)

Fig. 4 Different meshes used for mesh density study Artery-0.1mm, Stent 0.1mm (a);
          Artery 0.08mm, Stent -0.05mm (b)

Fig. 5 plots the radial displacement of the luminal surface for a default mesh and a mesh of the chosen element size.


a)   b)

Fig. 5 Radial displacement of artery inside surface default mesh (a); and refined mesh (b)

3. RESULTS AND DISCUSSION

The following section discusses the results of investigations in the form of plots, tables and graphs.
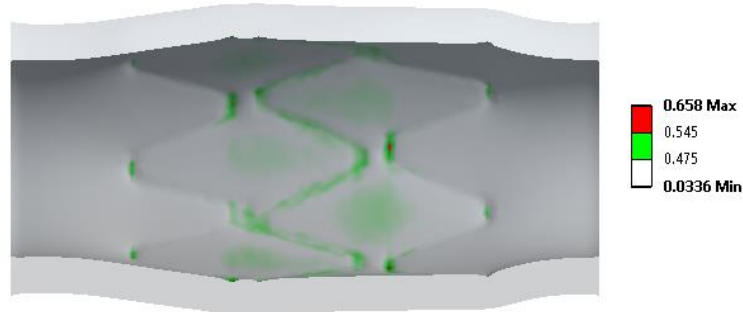
Fig. 6 VMS distribution on artery luminal surface (Class I-0.545MPa to 0.658MPa and Class III- 0.475MPa to 0.545MPa) for Stent S at 2MPa inflation pressure (legend unit, MPa)
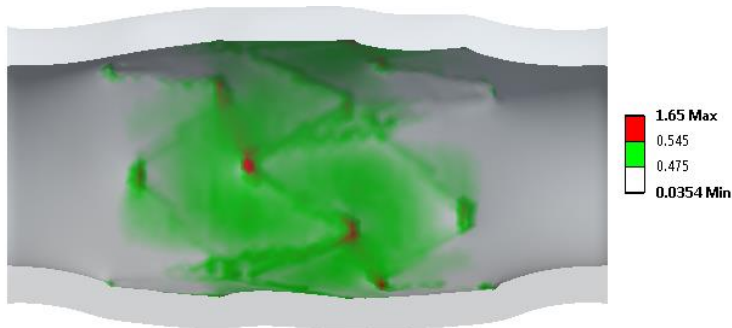

Fig. 7 VMS distribution on artery luminal surface (Class I-0.545MPa to 1.65MPa and Class III- 0.475MPa to 0.545MPa) for Stent T at 2MPa inflation pressure (legend unit, MPa)

Table 5 Percentage of luminal surface of arterial tissues subjected to class III critical stress level

| Stent	Percentage of luminal surface above 475kPa at 2MPa inflation pressure
Stent S	0.27
Stent T	9.1

We have observed VMS concentration predominantly on the internal surface of artery segments, with a diminishing stress across section, suggesting a large percentage volume of the artery remaining much below non-physiological stress (above class III). Figs. 6 and 7 show contour plots of VMS distribution on the inside surface of artery for Stent S and Stent

T, respectively. It suggests that the artery segment in line with the stent crown is the area more susceptible for restenosis (Class I stress level). Stent S induced considerably a smaller area of critical stress region (Table 5). This can be attributed to a lower stent/artery contact area (3.77mm^2) compared to that of Stent T (5.5mm^2). For Stent S, the critical stress region is observed along the stent-artery contact region while majority of the stented surface remained much below the critical stress (between 0MPa-0.475MPa). For Stent T, approximately the entire stented region is subjected to critical stress state (between 0.475MPa-1.65MPa).
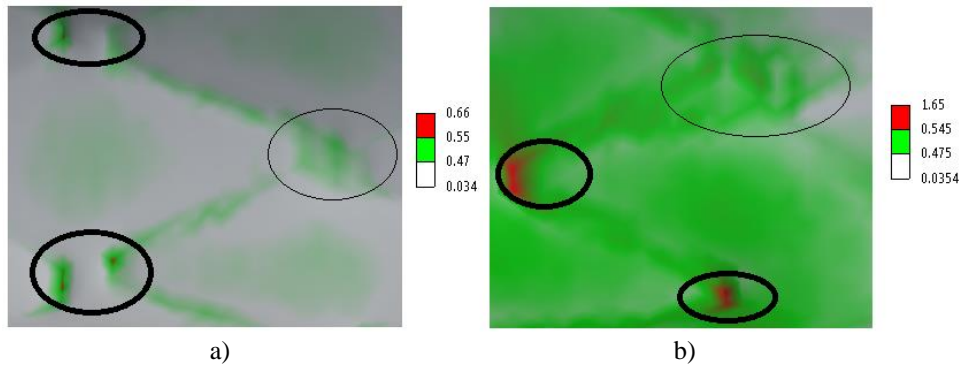
Fig. 8 Distribution of class I and class III stress level. Stent crown unbound by link (thick circle) and stent crown bound by link (thin circle) for Stent S(a), Stent T (b)

A closer look at the location of critical stress level (Fig. 8) shows that higher VMS areas (Class I) are essentially located near the stent crowns unbound by connecting links, while near the bound crown a more distributed stress pattern is observed. This can be attributed to the fact that the stent crown unbound by links is more likely to open up and penetrate into the artery during expansion which is also evident from Fig. 9 showing prolapse of arterial tissues through the stent struts at these locations.
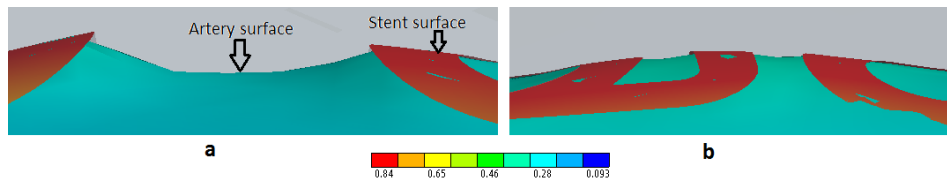

Fig. 9 Artery and stent surface after expansion, indicating larger tissue prolapse through stent struts at location without link (a) and no prolapse at location with link (b) (legend unit, mm)

A plot of VMS gradient on the inside surface of the artery along artery length (Figs. 10 and 11) suggests the existence of certain high stress gradient points. Plot essentially shows the VMS gradient calculated along two random longitudinal paths (path 1 and path 2) on the internal surface of the artery. Incidentally, path 1 passes through the location where it encounters the stent crown unbound by link. Interestingly, the locations of high VMS gradient happened to be on path 1 promptly suggesting consequence of tissue

prolapse as discussed previously. Stent T induced a comparatively higher stress gradient (5MPa/mm) in comparison with Stent S (3MPa/mm). In Stent T, the links are connected at the center of the stent struts unlike in Stent S where the links are connected to the stent crown, which would have resulted in a greater number of high gradient points for Stent T. High stress and stress gradient stimulate the regrowth of arterial tissue through the stent strut. This phenomenon is called re-stenosis which makes revascularization inevitable.
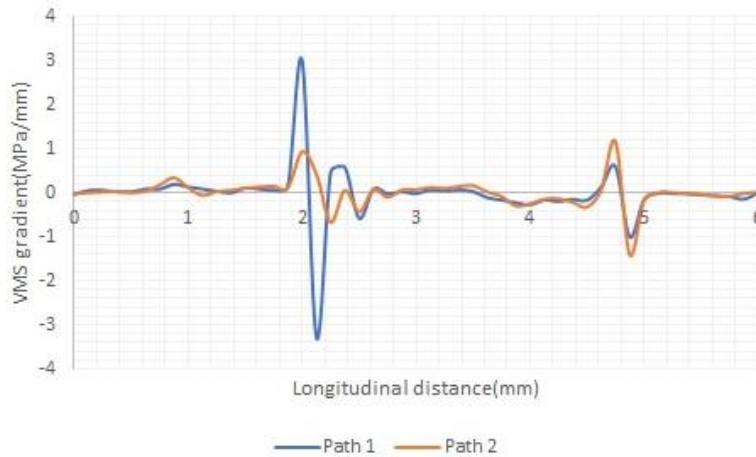

Fig. 10 VMS gradient on artery inside surface along artery length for Stent S at 2MPa inflation pressure
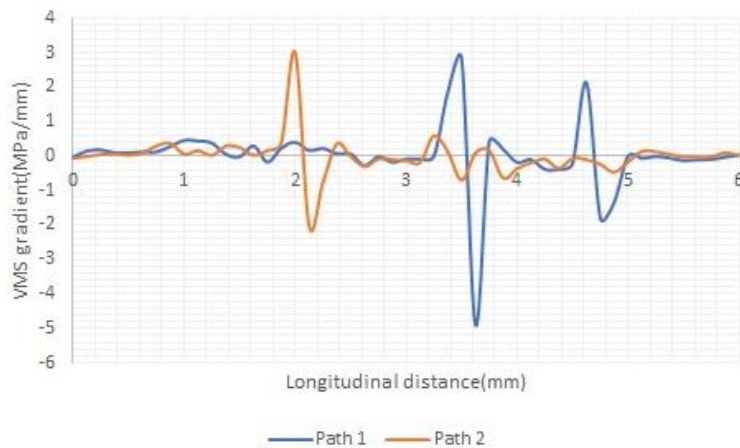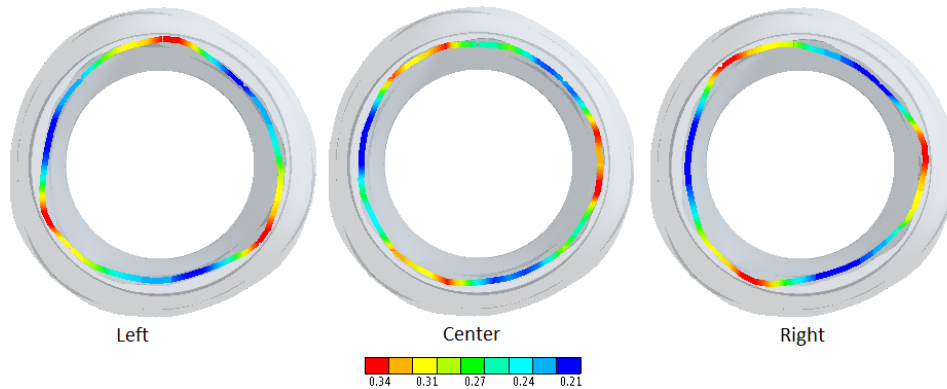

Fig. 11 VMS gradient on artery inside surface along artery length for Stent T at 2MPa inflation pressure

The following plots (Figs. 12 and 13) show radial displacement of the arterial inside surface at three circular sections at left, right and central region stented portion of the artery. Incidentally, the left and right sections happened to pass through the linked region while the

central section passes through a region devoid of links. Plots indicates more uniform (circular) displacement for the central section compared to the left and right sections. At the left and right regions, maximum displacement is observed at the locations of links (2 diametrically opposite locations for Stent S and 3 locations at 120^0 apart for Stent T). This finding suggests the influence of the links in achieving higher radial displacements.
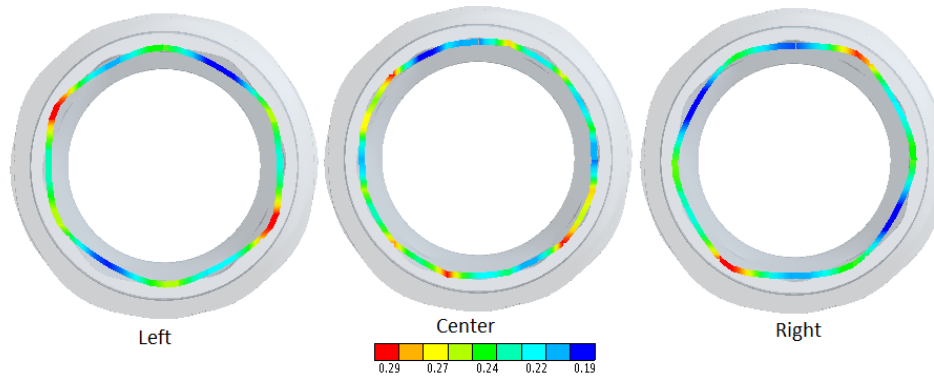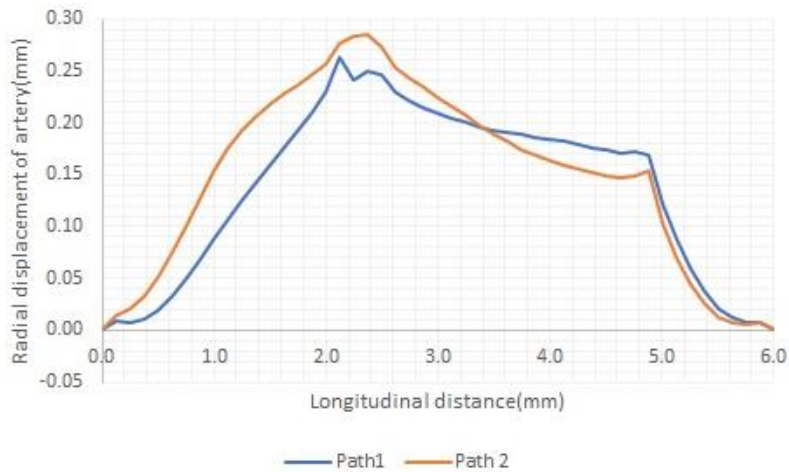

Fig. 12 Radial displacement of arterial inside surface at left, center and right sections for Stent S at 2MPa inflation pressure (legend unit, mm)
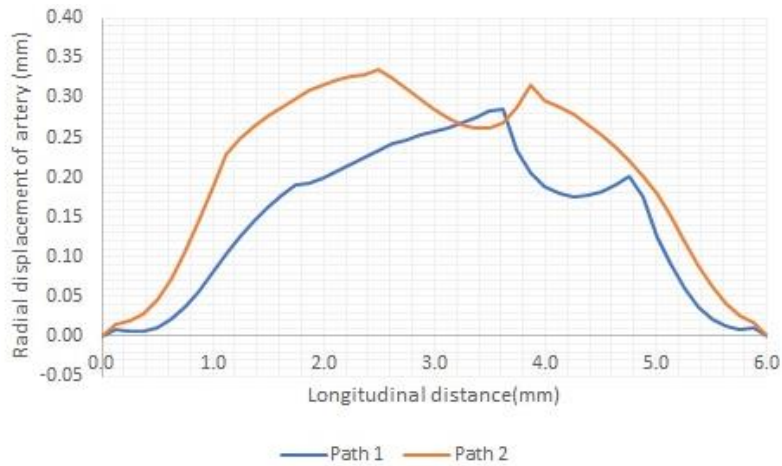

Fig. 13 Radial displacement of arterial inside surface at left, center and right sections for Stent T at 2MPa inflation pressure (legend unit, mm)

For Stent S, the difference between maximum and minimum radial displacement is found to be 0.11mm for both the left and right sections while in the central section the difference is found to be 0. 05mm. For Stent T the difference is found to be 0.15mm at left ,0.13mm at right and 0.05mm at central section, thus rightfully suggesting the necessity of a closed cell stent design (more links) to achieve circular expansion [25].

Fig. 14 Variation radial displacement of artery inside surface along artery length for Stent S at 2MPa inflation pressure
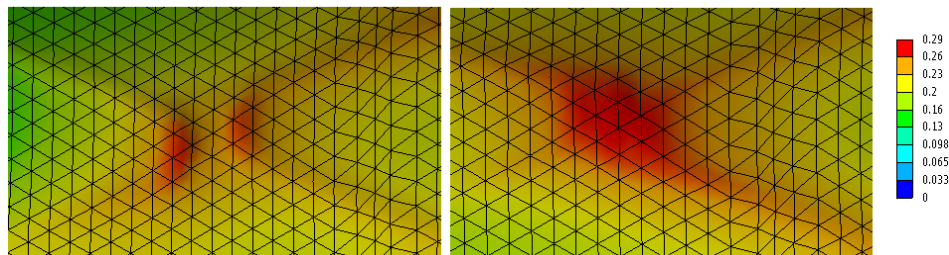

Fig. 15 Variation radial displacement of artery inside surface along artery length for Stent T at 2MPa inflation pressure

Non-uniformity of radial displacement is observed along longitudinal direction as well for both stent designs. The plot (Figs. 14 and 15) shows the variation of radial displacement of the arterial inside surface along longitudinal direction of the artery. Radial displacement is plotted through two longitudinal paths, path 1 and path 2, so that these paths pass through the locations of the stent crown. Interestingly, path 2 encountered a pair of stent crown bound by the links. The plots suggest that the radial displacements increase gradually from the ends of the artery through the stented region. The maximum displacement value is located near the stent crown for both path 1 (0.26 mm) and path 2 (0.29 mm) for Stent S. Larger maximum radial displacement for path 2 propose the influence of the link. The links

not only achieved larger maximum displacement at this location but also contributed to higher displacement in the vicinity of the stent crown. Similar trend is observed for Stent T. For Stent T the maximum radial displacements observed are 0.29 mm for path 1 and 0.34 mm for path 2.

Fig. 16 below takes a closer look on displacement of the luminal surface near the stent crown with and without link for Stent S. It is observed that the stent crown unbound by links is bound to misalign when expanded and may result in twisting of the artery surface damaging endothelium surface.

Fig. 16 Radial displacement of arterial inside surface near stent crown without link (a); and with link (b) for Stent S (legend unit, mm)

4. CONCLUSION, LIMITATIONS AND SCOPE FOR FUTURE STUDY

This study investigates the performance of two commercial stent designs inside the normal artery particularly highlighting an induced stress field, an arterial displacement pattern and the factor affecting it. The result suggests that the link contributes crucially to maintaining a uniform stress field in the stented region. The presence of the link reduced the VMS gradient and maintained uniform arterial displacements as well. Uniformity of expansion is greatly affected near the stent crown unbound by link. The link also contributed to lesser tissue prolapse and lesser misalignment. The results suggest that stent designs with bound stent crowns can induce diffused stress pattern and uniform arterial displacement. It can also result in minimal arterial distortions thereby minimizing detrimental effect arising from non-native biomechanical environment on tissues.

3-Dimensional idealized geometry is used in this investigation with simplifications (round edges of the strut are avoided). Using realistic models directly for investigation can simulate the effect of surface irregularities caused by drug coating and crimping process. Idealized artery geometry used here can certainly help in differentiating performance of different designs but realistic stenosed artery obtained from imaging techniques such as Intra Vascular Ultra Sound IVUS [26] can improve the investigation results in terms of applicability of stent design for specific lesion type. The boundary conditions used for avoiding rigid body motions of artery and stents in this study are simplified. It is assumed that few nodes of central stent cells move only in radial direction. In actual case, all the points on stent surface move in longitudinal and tangential directions. Hence, the boundary conditions that are more realistic can improve the validity of numerical investigation and translation of numerical inferences into clinical applications will be accomplished. Though we reported the values of stress and stress gradients in this study, these values are to be

considered with almost care as mesh density study suggests considerable variation in maximum Von Mises Stress for different mesh sizes. Nevertheless, the pattern of stress and stress gradient can be certainly relied upon.

REFERENCES

1. Mathers, C.D., Boerma, T., Ma Fat, D., 2009, *Global and regional causes of death*, Br. Med. Bull., 92(1), pp. 7-32.
2. Mozaffarian, D., 2016, *AHA Statistical Update Heart Disease and Stroke Statistics — 2016 Update A Report From the American Heart Association*, Circulation, 133(4), pp. e38-e360.
3. Whittaker, D.R., Fillinger, M.F., 2006, *The Engineering of Endovascular Stent Technology: A Review,* Vasc. Endovascular Surg., 40(2), pp. 85-94.
4. Ramakrishnan, S., Mishra, S., Chakraborty, R., Sarat Chandra, K., Mardikar, H.M., 2013, *The report on the Indian coronary intervention data for the year 2011 e National Interventional Council*, Indian Heart J., 65(5), pp. 518-521.
5. Timmins, L.H., 2011, *Increased artery wall stress post-stenting leads to greater intimal thickening*, Lab. Investig., 91(6), pp. 955–67.
6. Zahedmanesh, H., Cahill, P.A., Lally, C., 2012, *Vascular Stent Design Optimisation Using Numerical Modelling Techniques*, Applied Biological Engineering – Principles and Practice, pp. 237–260.
7. Stoeckel, D., 2002, *A Survey of Stent Designs,* Min Invas Ther Allied Technol, 11(4), pp. 137–147.
8. Rogers, C., 1999, *Balloon-Artery Interactions During Stent Placement: A Finite Element Analysis Approach to Pressure, Compliance, and Stent Design as Contributors to Vascular Injury,* Circ. Res., 84, pp. 378–383.
9. Early, M., Kelly, D.J., 2010, *The role of vessel geometry and material properties on the mechanics of stenting in the coronary and peripheral arteries,* Proc. Inst. Mech. Eng. H., 224(3), pp. 465–476.
10. De Beule, M., 2008, *Realistic finite element-based stent design: The impact of balloon folding*, J. Biomech., 41(2), pp. 383-389.
11. Mitra, A.K., Agrawal, D.K., 2006, *In stent restenosis: bane of the stent era*, J Clin Pathol, 59, pp. 232–239.
12. Kornowski, R.A.N., Hong, M.U.N., Tio, K.F.O., Bramwell, O., Wu,H., Leon, M.B., 1998, *In-Stent Restenosis : Contributions of Inflammatory Responses and Arterial Injury to Neointimal Hyperplasia,* J. Am. Coll. Cardiol., 31(1), pp. 224-230.
13. Schwartz, R.S., Huber, K.C., Murphy, J.G., Edwards, W.D., Camrud, A.R., Vlietstra, R.E., Holmes, D.R., 1992, *Restenosis and the Proportional Neointimal Response to Coronary Artery Injury : Results in a Porcine Model*, J. Am. Coll. Cardiol., 19(2), pp. 267-274.
14. Azaouzi, M., Makradi, A., Belouettar, S., 2013, *Numerical investigations of the structural behavior of a balloon expandable stent design using finite element method*, Comput. Mater. Sci., 72, pp. 54-61.
15. Bukala, J., Kwiatkowski, P., Malachowski, J., 2016, *Numerical analysis of stent expansion process in coronary artery stenosis with the use of non-compliant balloon*, Biocybern. Biomed. Eng., 36(1), pp. 145-156.
16. David Chua, S.N., Mac Donald, B.J., Hashmi, M.S.J., 2003, *Finite element simulation of stent and balloon interaction,* J. Mater. Process. Technol., 143–144(1), pp. 591-597.
17. Bedoya, J., Meyer, C.A., Timmins, L.H., Moreno, M.R., Moore J.E., 2006, *Effects of stent design parameters on normal artery wall mechanics*, J. Biomech. Eng., 128(5), pp. 757-765.
18. Martin, D., Boyle, F., 2013, *Finite Element Analysis of Balloon-Expandable Coronary Stent Deployment : Influence of Angioplasty Balloon Configuration*, Int. J. Numer. Meth. Biomed. Engng., 29(11), pp. 1161-1175.
19. Raut, B.K., Patil,V.N., Cherian, G., 2017, *Coronary artery dimensions in normal Indians,* Indian Heart J., 69(4), pp. 512-514.
20. Migliavacca, F., Petrini, L., Colombo, M., Auricchio, F., Pietrabissa, R., 2002, *Mechanical behavior of coronary stents investigated through the finite element method,* J. Biomech., 35(6), pp. 803-811.

21. Migliavacca, F., Petrini, L., Montanari, V., Quagliana, I., Auricchio, F., Dubini, G., 2005, *A predictive study of the mechanical behaviour of coronary stents by computer modelling,* Med. Eng. Phys., 27(1), pp. 13-18.
22. Lally, C., Dolan, F., Prendergasr, P.J., 2005, *Cardiovascular stent design and vessel stresses: A finite element analysis,* J. Biomech., 38(8), pp. 1574-1581.
23. Pant, S., Bressloff, N.W., Limbert, G., 2012, *Geometry parameterization and multidisciplinary constrained optimization of coronary stents,* Biomech. Model. Mechanobiol., 11(1-2), pp. 61-82.
24. GU, L., Zhao, S., Froemming, S.R., 2012, *Arterial Wall Mechanics and Clinical Implications After Coronary Stenting: Comparisons of Three Stent Designs*, Int. J. Appl. Mech., 4(2), 1250013.
25. Schillinger, M., Gschwendtner, M., Reimers,B., Trenkler, J., Stockx, L., Mair, J., MacDonald, S., Karnel, F., Huber, K., Minar, E., 2008, *Does carotid stent cell design matter?*, Stroke, 39(3), pp. 905-909.
26. Buccheri, D., Piraino, D., Andolina, G., Cortese, B., 2016, *Understanding and managing in-stent restenosis : a review of clinical data, from pathogenesis to treatment,* J. Thorac. Dis., 8(3), pp. 1150-1162.